A P-type Modified Quadratic Gain Buck-Boost Converter for DC Microgrids

P. Raviteja, *Graduate Student Member, IEEE,* B. L. Narasimharaju, *Senior Member, IEEE,* and S. V. K. Naresh, *Member, IEEE*

***Abstract*— A p-type modified quadratic gain buck-boost (PMQBB) converter is proposed in this paper. PMQBB converter topology evolution is based on the integration of a modified quadratic boost configuration with the p-type converter structure. Both of the inductors are in continuous conduction mode (CCM). The proposed PMQBB converter's key features include a reduced component count, lower order, high voltage gain, and continuous input current. The proposed PMQBB converter exhibits a buck capability at a duty ratio D ≤ 0.2929. This paper provides a comprehensive description of the PMQBB converter, including its steady-state analysis, operating modes, and analysis of semiconductor voltage and current stress. To emphasize the PMQBB converter, a detailed comparative study is presented. A 40/400 V, 300 W hardware prototype is tested to authenticate the converter's performance. The experimental outcomes validate the superior performance and efficiency of the PMQBB converter, highlighting its suitability for high-gain applications.**

Link to graphical and video abstracts, and to code: https://latamt.ieeer9.org/index.php/transactions/article/view/9621

Index Terms*— *Buck-Boost converter, DC-DC non-isolated converter, DC micro grid, High voltage gain, Quadratic Boost.

I. Introduction

NOWADAYS, the growing energy demand, driven by increased energy utilization, has led to a rise in energy generation [1]. The United Nations Development Programme (UNDP)'s Sustainable Development Goal 7 aims to ensure access to affordable, reliable, and sustainable energy for all. Supporting this goal, the United Nations Economic Commission for Latin America and the Caribbean (ECLAC) 2030 Agenda highlights the importance of clean energy technologies in driving economic and environmental transformation. The integration of DC-DC converters is crucial for these Conventional energy sources, such as fossil fuels contribute to environmental pollution and accelerate the depletion of natural resources. To mitigate these issues, using non-conventional energy sources (NCES) like solar power, wind energy, and fuel cells offers a sustainable solution. NCES to regulate voltage levels, making them suitable for various applications, including DC microgrids, LED lighting, and electronic devices. These converters can function as buck, boost, and buck-boost configurations [2] to ensure the correct voltage for optimal performance concerning applications. In the literature, numerous DC-DC converter configurations have been introduced based on isolated and non-isolated converters. In these, the first group of isolated converters uses transformers, and a high voltage gain can be achieved by adjusting the coil turns of the isolation transformer [3], eliminating the need for a high-duty cycle.

However, this approach has several limitations. Firstly, the inclusion of a transformer increases the cost and size of the converter, resulting in a reduction in power density. Furthermore, transformer coil leakage inductance generates a residual current. This results in improper switching, which in turn causes excessive voltage stress on the switch. These considerations highlight that transformer-less converters are the more suitable option for applications where isolating the output from the input is not required.

The aforementioned drawbacks are resolved by employing non-isolated DC-DC converters. These converters have improved efficiency with high voltage gain and low voltage stress, all while being at a lower cost, reduced size, and lighter weight. Although conventional boost converters [4] have a simple structure with fewer components, they are unsuitable for high-power applications because semiconductor components endure substantial voltage stress. Non-isolated converters are generally classified into two types: coupled inductors and non-coupled inductors. Many high-step-up converters based on coupled inductors [5] have been developed, leveraging a higher turn ratio to achieve a significant voltage gain. However, in presence of leakage inductance in coupled inductors can lead to voltage spikes, which increase the voltage stress on the switches, similar to the issues in isolated converters. To address this issue, additional snubber circuits are employed. However, their inclusion increases the converter's overall cost and size. Non-coupled inductor configuration types are capable of achieving high voltage gain with fewer magnetic components. In cascade boost converters [6], [7], the voltage gain ratio is determined by the combined gains of each stage. However, this multistage design can lead to reduced efficiency and is inherently complex. Numerous techniques have been investigated in the literature to enhance voltage gain, including switched capacitor [8], SEPIC [9], voltage multiplier [10], active switched inductor [11], and hybrid switched inductor [12]. Nevertheless, the voltage gain achieved remains relatively modest; switched inductor and switched capacitor topologies experience high current stress. Additionally, voltage multipliers and converters based on voltage lift techniques tend to have increased component counts and reduced efficiency. To overcome the issue of low voltage gain, a

The associate editor coordinating the review of this manuscript and approving it for publication was Pedro Machado de Almeida (*Corresponding author: P. Raviteja*).

P. Raviteja, and B. L. Narasimharaju are with the National Institute of Technology Warangal, Hanamkonda, Telangana, India (e-mails: pr22eer1r08@student.nitw.ac.in, and blnraju@nitw.ac.in).

S. V. K. Naresh is with SRM University-AP, Amaravati, Andhra Pradesh, India (e-mail: naresh.s@srmap.edu.in).

multistage switched inductor configuration integrated with a switched capacitor was introduced in [13], although this approach leads to an increased number of components. An effective solution to these constraints is achieving a high voltage gain at a low duty cycle with less component count. A non-isolated DC-DC converter with a three-switching state-based split-duty design is presented in [14]. To avoid extended conduction periods in the interleaved switches, this design includes one extra switch. Additionally, the inclusion of the extra switch necessitates an additional driver board, increasing the system's complexity and cost. The converters discussed in [15] and [16] introduce different approaches to achieve high gain with a low duty ratio. While the converter in [15] delivers enhanced voltage gain, it experiences significantly higher peak switch current stress, and the component count is high. Additionally, operating at low duty ratios adds to the control complexity. Quadratic boost converters [17]-[25] are becoming increasingly popular due to their capability to achieve a high conversion ratio while maintaining a low-duty cycle. However, quadratic boost converters [19] - [24] have certain limitations, such as a higher element count, reduced effectiveness index [25], lower voltage gain, and an increased system order due to a larger number of energy storage components.

To address the aforementioned limitations of converters while retaining their advantages, the PMQBB converter has been designed. The PMQBB converter topology is derived from the modified quadratic boost converter, which is integrated into the p-type structure. The proposed PMQBB converter exhibits notable advantages, including a simplified structural design, high voltage gain, reduced count of energy storage elements, and the ability to sustain continuous input current. The paper is organized as follows: Section II provides the principle of operation and analysis of the proposed PMQBB converter, switch-diode stresses, parameter design, efficiency analysis, control performance, and power loss calculation. Section III provides a comparative analysis of the proposed PMQBB converter against other similar converters found in the literature. Section IV discusses the experimental evaluation of the PMQBB converter's performance metrics. Section V reports discussion on Advantages and Limitations, while Section VI concludes the paper by highlighting the key contributions of this state-of-the-art work.

II. Principle Of Operation And Analysis Of Proposed PMQBB

Fig. 1. depicts the proposed PMQBB converter. This converter features has two capacitors (C_0, C_1), two diodes (D_0, D_1), two inductors (L_1, L_2), and two switches (S_1, S_2). The proposed PMQBB converter operates in continuous conduction mode (CCM). For the sake of simplicity in analyzing the converter in CCM, all the devices used in the converter are assumed to be ideal. The proposed PMQBB converter operates in two modes, as shown in Fig.2. The operational waveforms of the PMQBB converter are presented in Fig. 3. They include gate signals of switches S_1 and S_2, voltages and currents of inductors L_1 and L_2, voltage across diodes D_1, and switch voltages of S_1 and S_2.

A. Operating Modes:

Mode-1:

As shown in Fig. 2 (a), this mode is initiated at $t=t_0$. In mode I, the diodes D_0 and D_1 are in the OFF state, and the S_1 and S_2 switches are turned ON. The input DC source V_{in} charges inductors L_1 and L_2 via capacitor C_1, while capacitor C_0 delivers

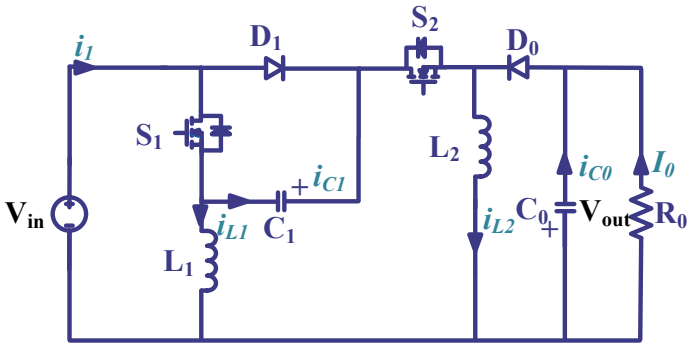

Fig. 1. Proposed PMQBB converter [26].

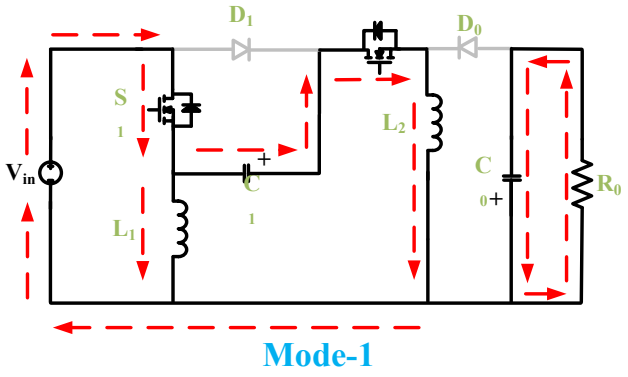

(a)

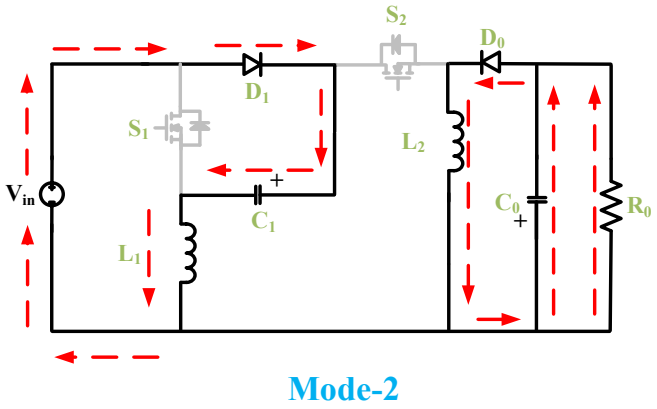

(b)

Fig. 2. Operating Modes of PMQBB converter (a) Mode-1 (b) Mode-2.

power to the output load R_0. Kirchhoff's voltage and current laws are used to obtain the following equations for Mode-1 in the duration of the t_0-t_1 interval.

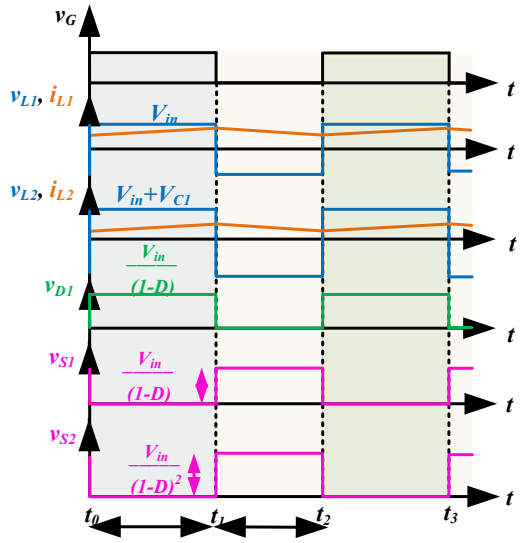

Fig. 3. Key operating waveforms of PMQBB converter.

$$V_{L1} = V_{in}\ ;\ V_{L2} = V_{in}+V_{C1} \tag{1}$$

$$\left.\begin{aligned} i_{C1} &= C_1\left(\frac{dv_{C1}}{dt}\right) = -\,i_{L2} \\ i_{C0} &= C_0\left(\frac{dv_{C0}}{dt}\right) = -\,I_0 \end{aligned}\right\} \tag{2}$$

Mode-2:

As shown in Fig. 2 (b) (Mode 2), in this mode, the switches S_1 and S_2 are turned OFF at t=t_1, resulting in diodes D_0 and D_1 turning ON. The inductors L_1 and L_2 start discharging in contrast to the previous mode. In addition to supplying energy from the input DC source V_{in}, inductor L_1 discharges to charge Capacitor C_1. At the same time, inductor L_2 discharges to energize capacitor C_0 and provides power to the output load R_0.

Kirchhoff's voltage and current laws are used for obtaining the following equations from Mode-2 in the interval t_1-t_2.

$$V_{L1} = V_{in}\text{-}V_{C1}\ ; V_{L2} = -\,V_{out} \tag{3}$$

$$\left.\begin{aligned} i_{C1} &= C_1\left(\frac{dv_{C1}}{dt}\right) = i_{L1} \\ i_{C0} &= C_0\left(\frac{dv_{C0}}{dt}\right) = i_{L2}\text{-}I_0 \end{aligned}\right\} \tag{4}$$

The equations below are derived using the volt-second balance principle for inductors L_1 and L_2.

$$(V_{in})D+(-v_{C1})(1\text{-}D)=0 \tag{5}$$

$$(V_{in}+v_{C1})D+(-V_{out})(1\text{-}D)=0 \tag{6}$$

By solving equations (5) and (6)

$$V_{C1}=\frac{V_{in}}{1\text{-}D} \tag{7}$$

$$G\left(\frac{v_{out}}{v_{in}}\right)=\left(\frac{(2\text{-}D)D}{(1\text{-}D)^2}\right) \tag{8}$$

By using equation (7) output voltage gain of the proposed PMQBB converter is given as

Similarly, by applying the ampere-second balance to equations (2) and (4), the average currents through the inductors are determined as follows:

$$\left.\begin{aligned} I_{L1} &= \frac{I_0 D}{(1\text{-}D)^2} \\ I_{L2} &= \frac{I_0}{(1\text{-}D)} \end{aligned}\right\} \tag{9}$$

B. Analysis of Stresses on Switches and Diodes:

The voltage stress is the peak voltage across the semiconductor devices during their non-conduction mode of operation. By applying KVL to mode-1 in Fig. 2, the voltage stresses on D_1 and D_0 can be determined. Furthermore, voltage stresses on S_1 and S_2 can be determined by applying KVL to mode-2 in Fig.2. From the operating modes, stresses experienced by the semiconductor components in the proposed PMQBB converter can be expressed as follows:

$$V_{D1}= V_{C1}=\frac{V_{in}}{1\text{-}D}=\frac{V_{out}(1\text{-}D)}{(2\text{-}D)D}\ ;\ V_{D0} = V_{L2}+V_{out}=\frac{V_{in}(2\text{-}D)}{(1\text{-}D)^2}=\frac{V_{out}}{D}\ ;$$
$$V_{S1}= V_{C1}=\frac{V_{in}}{1\text{-}D}=\frac{V_{out}(1\text{-}D)}{(2\text{-}D)D};\ V_{S2}=\frac{V_{in}}{(1\text{-}D)^2}=\frac{V_{out}}{(2\text{-}D)D}\ ; \tag{10}$$

The current stress is the peak current flowing through the semiconductor devices during their conduction modes. By applying KCL and analyzing mode-1 in Fig. 2, the current stresses on S_1 and S_2 can be determined. Furthermore, the current stresses on D_1 and D_0 can be determined by applying KCL to mode-2 in Fig.2. The semiconductor elements' average and peak current stresses are provided by

$$I_{S1}=D(I_{L1}+I_{L2});\ I_{S2}=DI_{L2}$$
$$I_{D1}=(1\text{-}D)I_{L1};\ I_{D0}=(1\text{-}D)I_{L2} \tag{11}$$

$$\hat{I}_{S1}=(I_{L1}+I_{L2})+\left(\frac{\Delta I_{L1}+\Delta I_{L2}}{2}\right);\ \hat{I}_{S2}=I_{L2}+\left(\frac{\Delta I_{L2}}{2}\right)$$
$$\hat{I}_{D1} = I_{L1}+\left(\frac{\Delta I_{L1}}{2}\right);\ \hat{I}_{D0} = I_{L2}+\left(\frac{\Delta I_{L2}}{2}\right) \tag{12}$$

Where

$$\left.\begin{aligned} \Delta I_{L1} &= \left(\frac{V_{in}}{L_1}\right)\frac{D}{f_S} \\ \Delta I_{L2} &= \left(\frac{V_{in}+V_{C1}}{L_2}\right)\frac{D}{f_S} \end{aligned}\right\}$$

C. Parameter Design:

i) Design of Inductors:

Choosing appropriate inductors is crucial for DC microgrid applications. The required inductance value is influenced by key operating parameters, including the switching frequency (f_s), duty cycle (D), input voltage (V_{in}), and the specified ripple current ($\%x_L I_L$) limits. The ripple current approximation for inductors L_1 *and* L_2 is 20% to 40% ($\%x_{L1}$&$\%x_{L2}$) of the inductor average current. Additionally, the inductor L_2 design choice ensures that the converter remains in continuous conduction mode (CCM)

across all operating conditions. From equation (13), selected inductor values are L_1=1mH and L_2=3mH.

$$\left.\begin{aligned} L_1 &\geq \frac{V_{in}D}{(\%x_{L1})I_{L1}f_S} \geq \frac{V_{in}^2(2\text{-}D)D}{(\%x_{L1})(1\text{-}D)^2P_0f_S} \\ L_2 &\geq \frac{(V_{in}+V_{C1})D}{(\%x_{L2})I_{L2}f_S} \geq \frac{V_{in}^2(2\text{-}D)^2D^2}{(\%x_{L2})(1\text{-}D)^2P_0f_S} \end{aligned}\right\} \quad (13)$$

ii) Design of Capacitors:

As with inductors, the selection of the capacitor is based on factors such as the maximum allowable voltage ripple ($\%x_{C1}$ v_C) the capacitor's operating voltage, and the current it must handle the acceptable voltage ripple of 1% to 5% ($\%x_{C1}$ & $\%x_{C0}$) of the corresponding capacitor average voltage is used as the basis for the design of capacitors C_0 and C_1. From equation (14) selected capacitor values are C_1=22 µF and C_0=100 µF.

$$\left.\begin{aligned} C_1 &\geq \frac{I_{C1}D}{(\%x_{C1})V_{C1}f_S} \geq \frac{P_0(1\text{-}D)^2}{(\%x_{C1})(2\text{-}D)D\,V_{in}^2f_S} \\ C_0 &\geq \frac{I_{C0}D}{(\%x_{C0})V_{out}\,f_S} \geq \frac{P_0(1\text{-}D)^4}{(\%x_{C0})(2\text{-}D)^2D^2\,V_{in}^2f_S} \end{aligned}\right\} \quad (14)$$

D. Efficiency Analysis of Proposed PMQBB Converter Considering Parasitic Elements:

The performance evaluation of the converter is influenced by the parasitic elements present in the converter circuit. The proposed PMQBB converter equivalent circuit with element parasitics is illustrated in Fig.4.

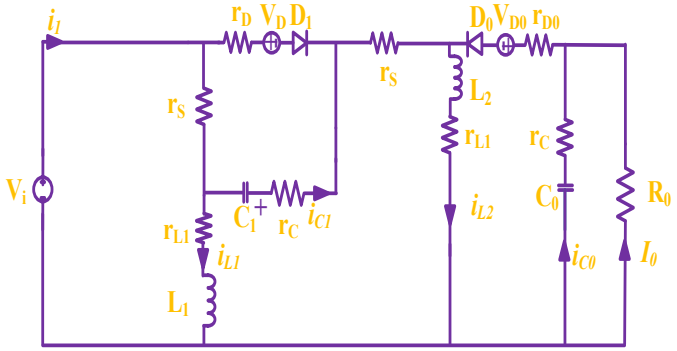

Fig. 4. Equivalent circuit of PMQBB converter with element parasitics.

$$V_{L1}=V_{in}-I_{L1}r_{L1}-(I_{L1}+I_{L2})r_s\}\rightarrow DT_S$$

$$V_{L1}=V_{in}-I_{L1}(r_c+r_D+r_{L1})-v_{C1}-V_D\}\rightarrow(1\text{-}D)T_S$$

$$V_{C1}=\frac{V_{in}}{1\text{-}D}-I_0(r_s+r_{L1})\left(\frac{D}{(1\text{-}D)^3}\right)-I_0(r_D+r_c)\left(\frac{D}{(1\text{-}D)^2}\right)-V_D$$

$$V_{out}=V_{C1}\left(\frac{(2\text{-}D)D}{1\text{-}D}\right)$$

$$V_{out\text{-}Parasitic}=\frac{V_{in}\left(\frac{(2\text{-}D)D}{(1\text{-}D)^2}\right)-V_D\left(\frac{(2\text{-}D)D}{1\text{-}D}\right)}{1+a\left(\frac{r_s+r_{L1}}{R_0}\right)+b\left(\frac{r_D+r_c}{R_0}\right)} \quad (15)$$

$$a=\frac{(2\text{-}D)D}{(1\text{-}D)^4},\ b=\frac{(2\text{-}D)D}{(1\text{-}D)^3}$$

$$\eta=\frac{1-V_D\left(\frac{(1\text{-}D)}{V_{in}}\right)}{1+a\left(\frac{r_s+r_{L1}}{R_0}\right)+b\left(\frac{r_D+r_c}{R_0}\right)} \quad (16)$$

E. Control Performance:

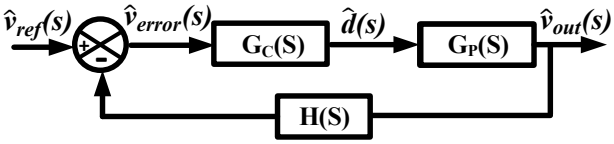

Fig. 5. Closed-loop control scheme of PMQBB converter.

By using the state-space averaging method, the PMQBB Converter performance is analyzed. In the steady-state analysis, two distinct operating modes are identified, each characterized by a unique set of differential equations.

The proposed PMQBB converter's small signal modeling is expressed through equations (17) and (18). The PMQBB topology includes L_1, L_2 inductors, and C_1 and C_0 capacitors, resulting in four state variables. Those are inductor currents i_{L1} (t), i_{L2} (t), and the capacitor voltages v_{C1} (t), v_{C0} $_{(t)}$. The control variable of the system is $d(t)$, while $v_{in}(t)$ and $v_{out}(t)$ represent input and output voltage variables, respectively.

The PMQBB converter state equations for the durations DT_s and $(1\text{-}D)T_s$ are written as

$$\xrightarrow{DT_S}\quad \frac{di_{L1}(t)}{dt}=\frac{v_{in}(t)}{L_1};\ \frac{di_{L2}(t)}{dt}=\frac{v_{in}(t)+v_{C1}(t)}{L_2};\ \frac{dv_{C1}(t)}{dt}=\frac{-i_{L2}(t)}{C};\ \frac{dv_{C0}(t)}{dt}=\frac{-I_0}{C_0}=\frac{-v_{C0}(t)}{R_0C_0}$$

$$\xrightarrow{(1\text{-}D)T_S}\quad \frac{di_{L1}(t)}{dt}=\frac{v_{in}(t)-v_{C1}(t)}{L_1};\ \frac{di_{L2}(t)}{dt}=\frac{-v_{out}(t)}{L_2};\ \frac{dv_{C1}(t)}{dt}=\frac{i_{L1}(t)}{C_1};\ \frac{dv_{C0}(t)}{dt}=\frac{i_{L2}(t)-I_0}{C_0}$$

$A=A_1D+A_2(1\text{-}D)$, $B=B_1D+B_2(1\text{-}D)$, $C=C_1D+C_2(1\text{-}D)$
A= average system matrix; A_1= State matrix during on state
A_2= State matrix during off state
B= input matrix; C= output matrix
X= state vector; U= input voltage
$X=-A^{-1}BU$

$$F=\{(A_1\text{-}A_2)X\}+\{(B_1\text{-}B_2)U\} \quad (17)$$

$$A_1=\begin{bmatrix} 0 & 0 & 0 & 0 \\ 0 & 0 & \frac{1}{L_2} & 0 \\ 0 & \frac{-1}{C_1} & 0 & 0 \\ 0 & 0 & 0 & \frac{-1}{R_0C_0} \end{bmatrix} \qquad B_1=\begin{bmatrix} \frac{1}{L_1} & \frac{1}{L_2} & 0 & 0 \end{bmatrix}^T$$

$$C_1=[0\quad 0\quad 0\quad 1]$$

$$A_2=\begin{bmatrix} 0 & 0 & \frac{-1}{L_1} & 0 \\ 0 & 0 & 0 & \frac{-1}{L_2} \\ \frac{1}{C_1} & 0 & 0 & 0 \\ 0 & \frac{1}{C_0} & 0 & \frac{-1}{R_0C_0} \end{bmatrix} \qquad B_2=\begin{bmatrix} \frac{1}{L_1} & 0 & 0 & 0 \end{bmatrix}^T$$

$$C_2=[0 \quad 0 \quad 0 \quad 1]$$

$$\begin{bmatrix} \frac{di_{L1}(t)}{dt} \\ \frac{di_{L2}(t)}{dt} \\ \frac{dv_{c1}(t)}{dt} \\ \frac{dv_{c0}(t)}{dt} \end{bmatrix} = \begin{bmatrix} 0 & 0 & 0 & 0 \\ 0 & 0 & \frac{1}{L_2} & 0 \\ 0 & \frac{-1}{C_1} & 0 & 0 \\ 0 & 0 & 0 & \frac{-1}{R_0C_0} \end{bmatrix} \begin{bmatrix} \hat{i}_{L1}(t) \\ \hat{i}_{L2}(t) \\ \hat{v}_{C1}(t) \\ \hat{v}_{C0}(t) \end{bmatrix} + \begin{bmatrix} \frac{1}{L_1} \\ 0 \\ 0 \\ 0 \end{bmatrix} \begin{bmatrix} \frac{1}{L_1} \\ \frac{1}{L_2} \\ 0 \\ 0 \end{bmatrix} v_{in}(t)$$

$$v_{c0}(t) = [0 \quad 0 \quad 0 \quad 1][i_{L1}(t) \quad i_{L2}(t) \quad v_{c1}(t) \quad v_{c0}(t)]^T$$

$$\begin{bmatrix} \frac{di_{L1}(t)}{dt} \\ \frac{di_{L2}(t)}{dt} \\ \frac{dv_{c1}(t)}{dt} \\ \frac{dv_{c0}(t)}{dt} \end{bmatrix} = \begin{bmatrix} 0 & 0 & \frac{-1}{L_1} & 0 \\ 0 & 0 & 0 & \frac{-1}{L_2} \\ \frac{1}{C_1} & 0 & 0 & 0 \\ 0 & \frac{1}{C_0} & 0 & \frac{-1}{R_0C_0} \end{bmatrix} \begin{bmatrix} \hat{i}_{L1}(t) \\ \hat{i}_{L2}(t) \\ \hat{v}_{C1}(t) \\ \hat{v}_{C0}(t) \end{bmatrix} + \begin{bmatrix} \frac{1}{L_1} \\ 0 \\ 0 \\ 0 \end{bmatrix} v_{in}(t)$$

$$v_{c0}(t)=[0 \quad 0 \quad 0 \quad 1][i_{L1}(t) \quad i_{L2}(t) \quad v_{c1}(t) \quad v_{c0}(t)]^T$$

Using (7) and (8), the average state equation of the PMQBB converter is written as

$$\begin{bmatrix} \frac{d\hat{i}_{L1}(t)}{dt} \\ \frac{d\hat{i}_{L2}(t)}{dt} \\ \frac{d\hat{v}_{C1}(t)}{dt} \\ \frac{d\hat{v}_{C0}(t)}{dt} \end{bmatrix} = \begin{bmatrix} 0 & 0 & \frac{-(1-d)}{L_1} & 0 \\ 0 & 0 & \frac{d}{L_2} & \frac{-(1-d)}{L_2} \\ \frac{(1-d)}{C_1} & \frac{-d}{C_1} & 0 & 0 \\ 0 & \frac{(1-d)}{C_0} & 0 & \frac{-1}{R_0C_0} \end{bmatrix} \begin{bmatrix} \hat{i}_{L1}(t) \\ \hat{i}_{L2}(t) \\ \hat{v}_{C1}(t) \\ \hat{v}_{C0}(t) \end{bmatrix} + \begin{bmatrix} \frac{1}{L_1} \\ \frac{d}{L_2} \\ 0 \\ 0 \end{bmatrix} \hat{v}_{in}(t) + [F]\hat{d} \tag{18}$$

$$v_{c0}(t) = [0 \quad 0 \quad 0 \quad 1][i_{L1}(t) \quad i_{L2}(t) \quad v_{c1}(t) \quad v_{c0}(t)]^T$$

$$F=\begin{bmatrix} \frac{d}{L_1}-\frac{d-1}{L_1} \\ \frac{d}{d-1}-\frac{dL_1(\frac{d}{L_1}-\frac{d-1}{L_1})}{(d-1)^2} \\ \frac{d^2}{(d-1)^3}-\frac{d^2L_1(\frac{d}{L_1}-\frac{d-1}{L_1})}{(d-1)^4} \\ \frac{d}{(d-1)^2}-\frac{dL_1(\frac{d}{L_1}-\frac{d-1}{L_1})}{(d-1)^3} \end{bmatrix} \hat{v}_{in}(t)$$

$$G_{vd}=\frac{\hat{v}_{out}}{\hat{d}}=C(SI-A)^{-1}[(A_1-A_2)X+(B_1-B_2)U]+(C_1-C_2)X$$

By applying small-signal perturbations to the converter and utilizing both steady-state and small-signal variables, the small-signal model of the PMQBB converter is derived. The proposed converter control to output transfer function is given in equation (19), by assuming no perturbations on the input side. As shown

$$G_{vd}\left(\frac{\hat{v}_{out}(s)}{\hat{d}(s)}\Big/\hat{v}_{in}(s)=0\right)=\frac{-5.73\times10^{27}\,s^3+1.31\times10^{32}\,s^2-1.268\times10^{35}\,s+8.243\times10^{38}}{2.267\times10^{23}\,s^4+4.25\times10^{24}\,s^3+2.678\times10^{30}\,s^2+4.894\times10^{31}\,s+2.782\times10^{35}} \tag{19}$$

in Fig.5, a PI controller is implemented to maintain a stable output voltage (V_o) despite these disturbances.

The controller adjusts constant output voltage through specific gain K_p=0.00000109, K_i=0.00331. The closed-loop stability of the proposed PMQBB is validated through Bode plots for both without a controller and with a controller configuration as indicated in Fig.6. (a), (b). Gain margin (G.M) and Phase margin (P.M) values are also represented in the respective plots, and also mention the stability of the system. The PI controller parameters are determined using the standard Ziegler–Nichols tuning method. This method provides a systematic way to achieve desired stability and dynamic performance.

F. Power Loss Calculation:

i) MOSFET Switch Power Loss Calculation:

Power losses in MOSFET switches result from both switching losses and conduction losses. Conduction losses in the switches arise from the on-state resistance of the switch. These conduction losses can be calculated as follows:

$$P_{SW\text{-}conduction}=I^2_{S1(rms)}R_{DS(on)}+I^2_{S2(rms)}R_{DS(on)} \tag{20}$$

The MOSFET switch switching losses can be given as

$$P_{SW\text{-}switching}=\frac{1}{2}(t_r+t_f)f_{sw}V_{DS1}I_{S1(pk)}+\frac{1}{2}(t_r+t_f)f_{sw}V_{DS2}I_{S2(pk)} \tag{21}$$

Here, f_{sw} is the switching frequency.

From equations (20) and (21), total MOSFET switch power losses are

$$P_{SW\text{-}Total}=P_{SW\text{-}conduction}+P_{SW\text{-}switching} \tag{22}$$

ii) Diode power loss calculation:

Diode power loss arises from the forward voltage drop (V_f) and the diode's internal resistance (R_d). This power loss can be represented by the following expression:

Power loss resulting from the forward voltage drop is

$$P_{D\text{-}FV}=V_{f1}I_{D1(avg)}+V_{f2}I_{D2(avg)} \tag{23}$$

Power loss due to the diode's internal resistance is

$$P_{D\text{-}Rd}=I^2_{D1(rms)}R_d+I^2_{D2(rms)}R_d \tag{24}$$

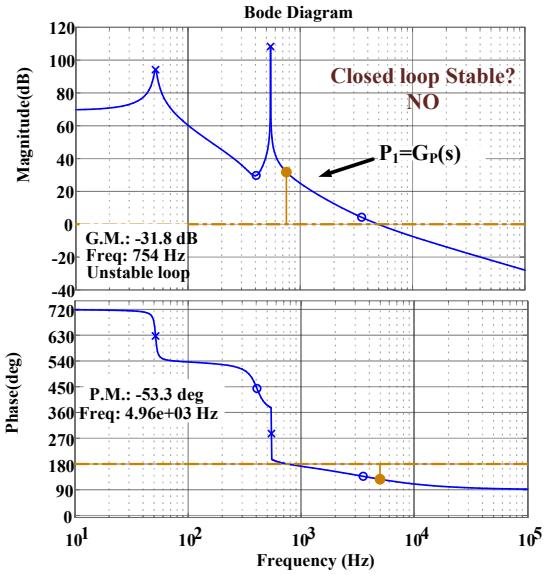

(a)

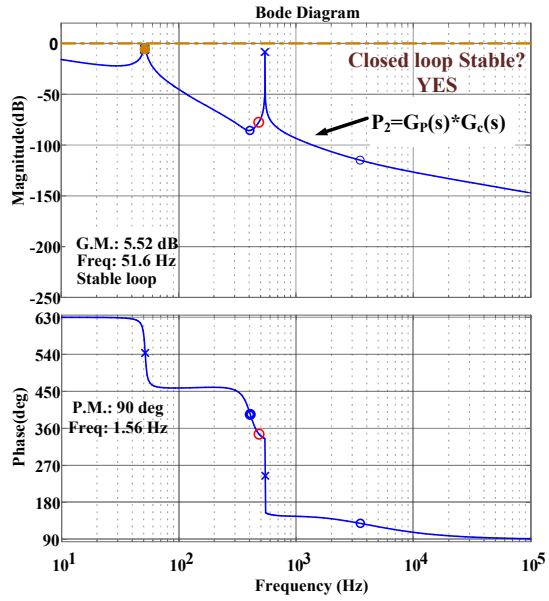

(b)

Fig. 6. Bode plot of proposed PMQBB: (a) Without a controller, (b) With a controller.

Here $I_{D(avg)}$&$I_{D(rms)}$ are represents average and r.m.s currents of the diodes.

Total diode power loss

$$P_{D\text{-}T}=P_{D\text{-}FV}+P_{D\text{-}Rd} \tag{25}$$

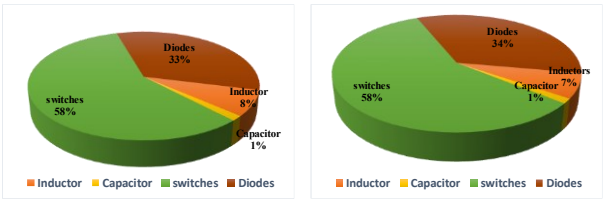

(a) (b)

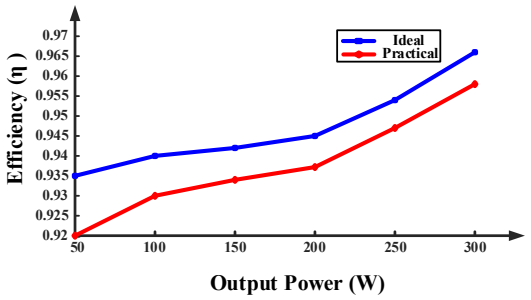

(c)

Fig. 7. PMQBB converter Loss distribution (a) theoretical, (b) practical, (c) Efficiency corresponding output power graph.

iii) Inductor power loss calculation:

Inductor power loss mainly results from copper loss and core loss. Copper loss in inductors can be represented by the following expression:

$$P_{in\text{-}cu}=I^2_{L1(rms)}R_{L1}+I^2_{L2(rms)}R_{L2} \tag{26}$$

Thus, R_L represents the equivalent series resistance (ESR) of the inductors, and I_{L1} denotes the root mean square (RMS) current flowing through the inductors.

Core losses are estimated as

$$P_{in\text{-}core}=KV_eB^x_{AC}f^y_{sw} \tag{27}$$

Total inductor power loss

$$P_{in\text{-}T}=P_{in\text{-}cu}+P_{in\text{-}core} \tag{28}$$

iv) Capacitor Power Loss Calculation:

In a capacitor, power loss is caused due to its internal resistance, and it can be expressed as

$$P_C=\left(I^2_{C1(rms)}+I^2_{C0(rms)}\right)R_C \tag{29}$$

Here, R_C is the internal resistance of capacitors, and $I_{C\,(rms)}$ is the r.m.s current flowing through capacitors.

From equations 20-29, the Total power loss can be calculated as follows:

$$P_T=P_{SW\text{-}Total}+P_{D\text{-}T}+P_{in\text{-}T}+P_C. \tag{30}$$

ESRs of inductors, capacitors, internal resistances of switches, and diodes are mentioned in Table II. Fig. 7 shows the theoretical, practical loss distribution, and efficiency variation concerning the change in output power of a proposed PMQBB converter.

II. COMPARATIVE ANLAYISIS

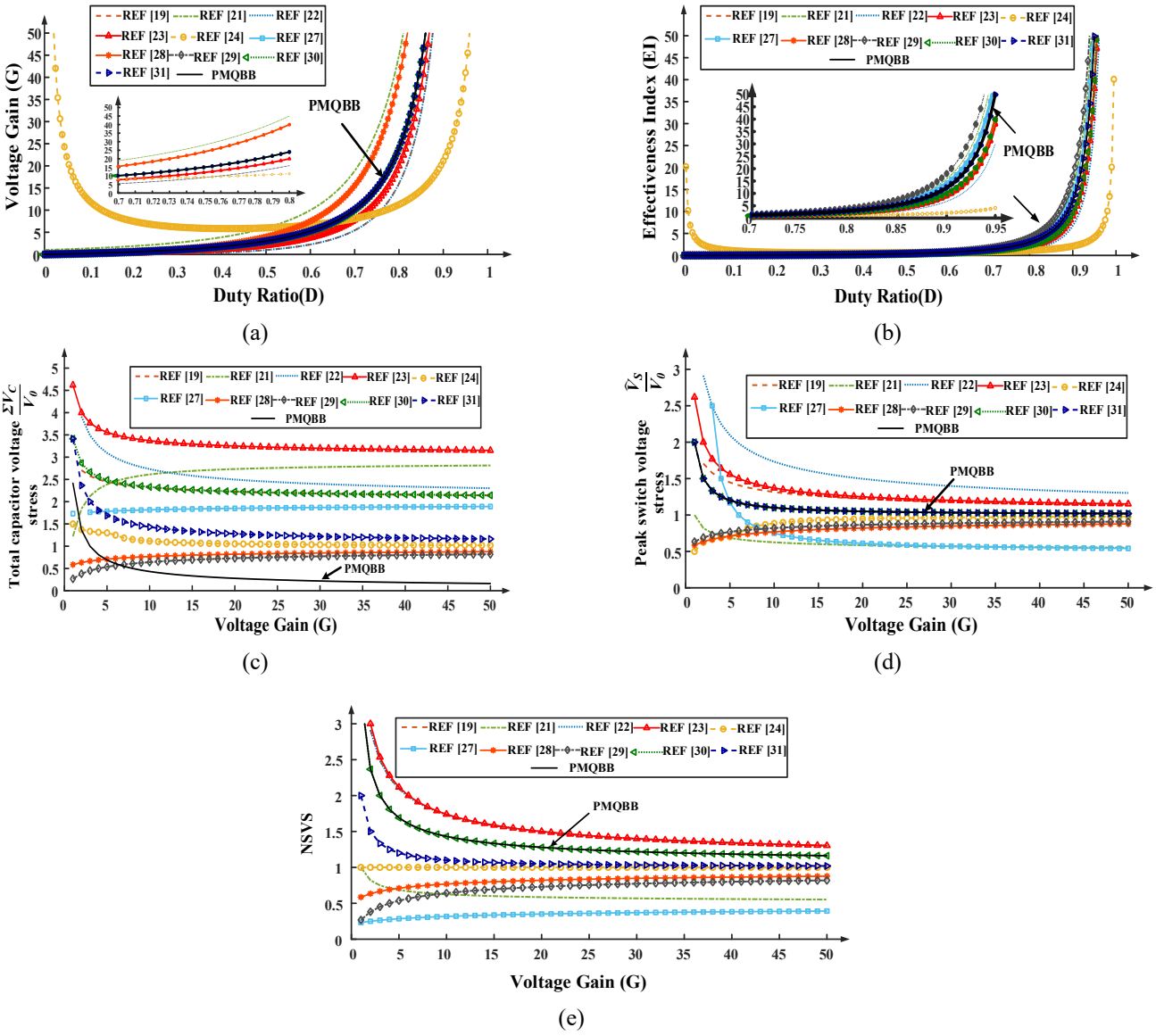

Fig. 8. Proposed PMQBB converter performance metrics comparison (a) G versus D, (b) EI versus D, (c) Total capacitor voltage Stress (TCVS) versus G, (d) Peak switch voltage stress (PSVS) versus G, (e) NSVS versus G.

The performance of the proposed PMQBB converter can be compared with other converters [19], [21]–[24], [27]–[31] documented in the literature to highlight its advantages, and the efficiency is presented in this section. Table I presents a detailed performance comparison evaluating parameters such as voltage gain, component count, order, power density, control complexity, total capacitor voltage stress (TCVS), peak switch voltage stress (PSVS), normalized switch voltage stress (NSVS), and operating conditions (f/P/η).The initially proposed PMQBB converter has been evaluated in terms of voltage gain in comparison to other converters. As demonstrated in Fig. 8(a), it is clear that the proposed PMQBB converter has the same gain as [28], [30], and [31], and achieves a higher voltage gain compared to the converters referenced in [19], [22]–[24]. At a duty ratio of 0.7, the proposed PMQBB converter achieves a voltage gain of 10, while converters [19], [22]–[24] provide only 5–8.The Effectiveness Index (EI) is the next parameter for comparison and is utilized to ensure consistency among the selected topologies. This demonstrates the voltage gain obtained per component, thereby effectively correlating the voltage gain with the total number of components. Fig. 8(b) shows that the PMQBB converter performance is superior to [19], [22]–[24], [28], and

[30]. Although converters [21] and [27] demonstrate high Effectiveness Index (EI), they employ 12 and 14 components, respectively, whereas the proposed PMQBB converter achieves comparable performance with only 8 components, indicating a more favorable trade-off between voltage gain and circuit complexity.The subsequent discussion of the parameter for comparison is total capacitor voltage stress (TCVS). In this aspect, PMQBB converter TCVS is the lowest among all compared converters, as illustrated in Fig. 8(c), which helps in reducing capacitor voltage ratings and improving reliability. The succeeding parameter for comparison is peak switch voltage stress (PSVS). Among all the converters, [21], [24], and [27]–[29] have superior performance than the PMQBB converter as shown in Fig. 8(d).

For instance, converter [27] shows a normalized PSVS of (1–D)/D, which is lower than that of PMQBB, but comes at the cost of significantly higher component count and control complexity. Further, the PMQBB converter is compared in terms of normalized switch voltage stress (NSVS), as depicted in Fig. 8(e). NSVS effectively corresponds to the overall equivalent stress encountered by the switches. The NSVS of the proposed PMQBB converter is higher than the converters in [21], [24], and [27]–[29], but is notably lower than those in [19], [22], and [23].Along with the parameters discussed above, the PMQBB converter is compared with other converters mentioned in Table I in terms of power density and control complexity. The PMQBB converter exhibits high power density due to fewer magnetic and switching elements and also features low control complexity attributed to its lower order (4). Furthermore, the PMQBB converter achieves an efficiency of 95.8% at 300 W and 50 kHz switching frequency, which is comparable to or better than most topologies except [27] and [30], which achieve 96.7% and 96.9% but at the expense of higher complexity.

The elaborate comparison shows that the proposed PMQBB converter excels across various indices. Further additional features of the proposed PMQBB converter are continuous input, fewer element count, the order of the system is lower, and efficiency is high. These attributes make the proposed PMQBB converter suitable for DC microgrid applications.

IV. Experimental Evaluation

A 400V/300W, 50 kHz prototype is fabricated for experimental evaluation of the PMQBB converter is as displayed in Fig. 9 (a) and Table. II shows the component specifications to develop the prototype of the PMQBB converter.

The prototype is tested with the input voltage of 40V with D=0.7, for which the output voltage V_{out} is 394V and the output current i_0 is 0.73A as shown in Fig. 10(a) at 95.8% operating efficiency. The gate pulse for S_1 and S_2 switches is given from the digital controller TMS320F28379D.

Fig. 10(b) illustrates the inductor currents and voltages, demonstrating the charging and discharging of the inductors corresponding to the switching operations of S_1 and S_2. Fig. 10(c) presents the voltage and current waveforms of the switches, which align well with the theoretical values. The switches experience peak voltage stresses of 133V and 440V, and peak current stresses of 9A and 2.9A, respectively. The diode and capacitor voltage waveforms are shown in Fig.10 (d) and (e). These are similar to the ideal case analytical values of the proposed PMQBB converter.

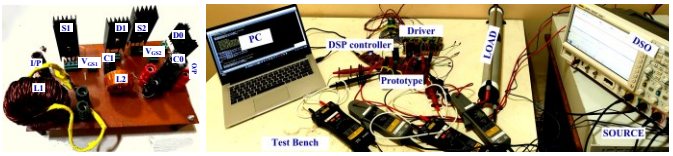

(a)

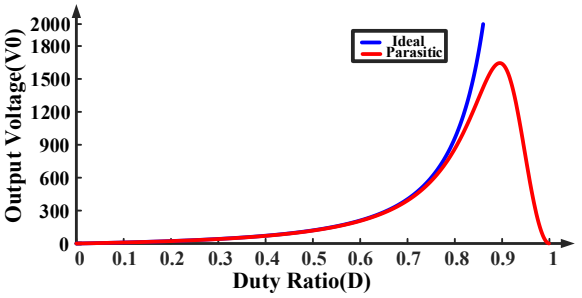

(b)

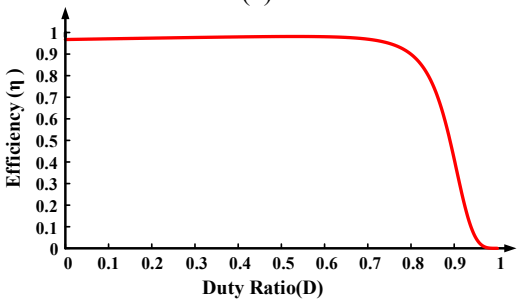

(c)

Fig. 9. PMQBB converter (a) Prototype & Experimental setup (b) $V_{0\text{-}Parasitic}$ and (c) η versus Duty ratio.

The PMQBB converter also has a buck converter characteristic capability at D≤0.2929. The PMQBB prototype is also tested with the input voltage of 40V at D=0.245, resulting output voltage of 29.5V and an output current of 1.45A as depicted in Fig. 10 (f). The control performance of the proposed PMQBB converter was evaluated under a sudden change in input voltage, varying from 40V-50V-40V-30V-40V. Fig. 11(a) presents the output voltage waveform corresponding to this step change operation. Fig. 11(b) shows the consistent voltage 400V waveform for the load variations from half load to full load and full load to half load. In both cases, the designed PI controller maintained the output voltage at 400V, regardless of fluctuations in input voltage and load current. Consequently, it can be concluded that the PMQBB converter exhibits excellent dynamic behavior with a response time of 72 milliseconds for input voltage variation and 58 milliseconds for load variation.

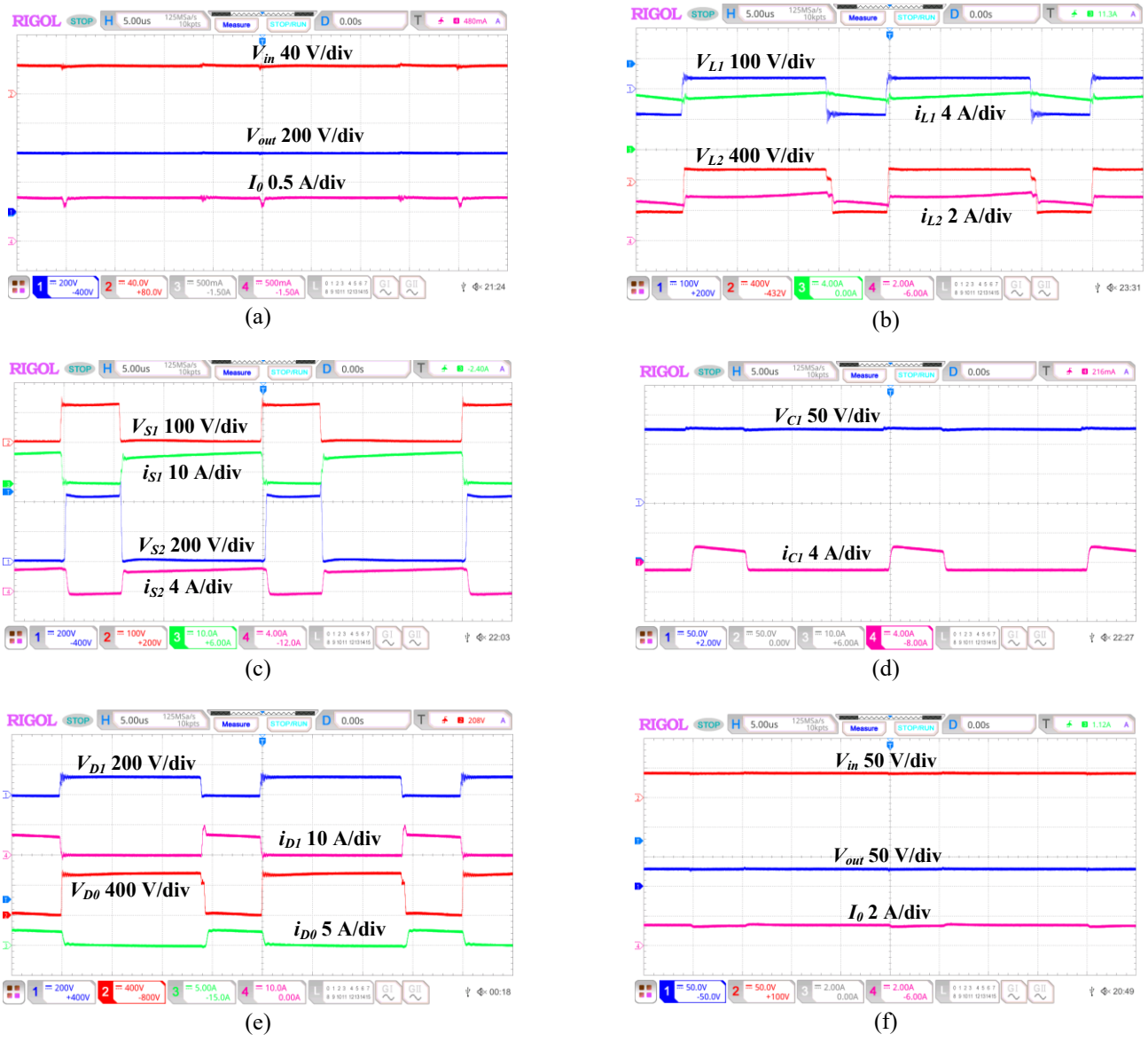

Fig. 10. Experimental results (a) input voltage (V_{In}), output voltage (V_{out}) and current (I_0) (b) Inductor voltages and currents (c) Switch voltages and currents (d)Capacitor C_1 voltage and currents (e) Diode D_1, D_0 voltages and currents (f)input voltage (V_{in}), output voltage (V_{out}) and current (I_0) in buck mode.

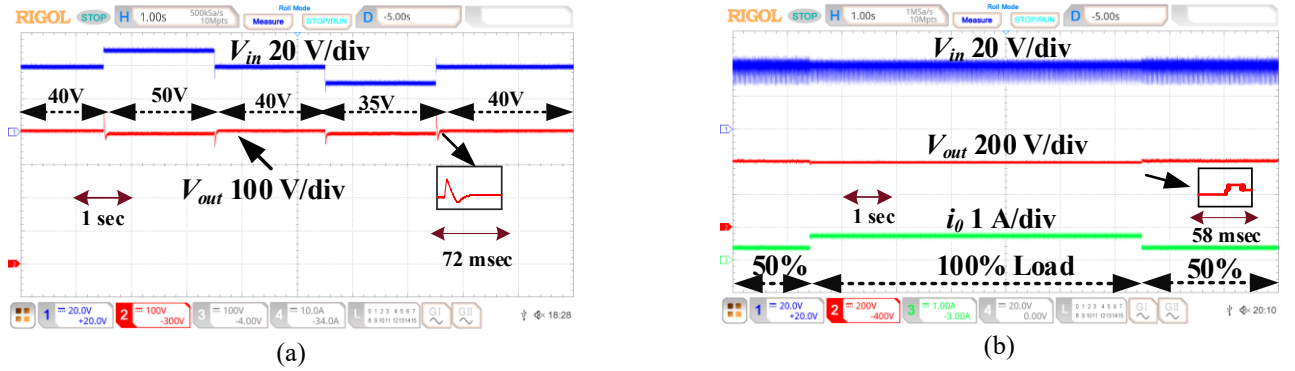

Fig. 11. PMQBB converter performance in closed loop: (a) sudden change in input voltage, (b) load change.

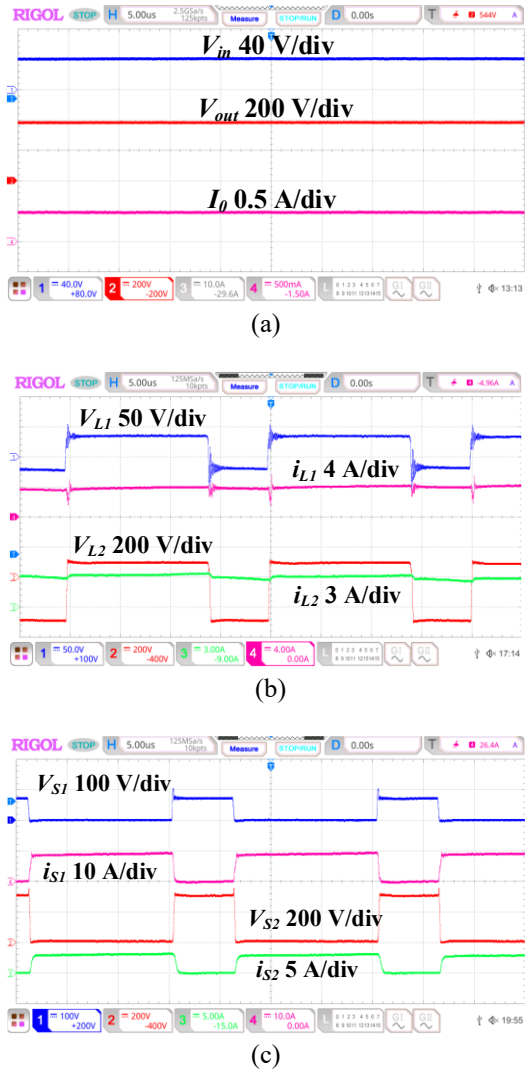

Fig. 12. Experimental results of 40V input 200W load (a) input voltage (V_{In}), output voltage (V_{out}), and current (I_0), (b) Inductor voltages and currents, (c) Switch voltages and currents

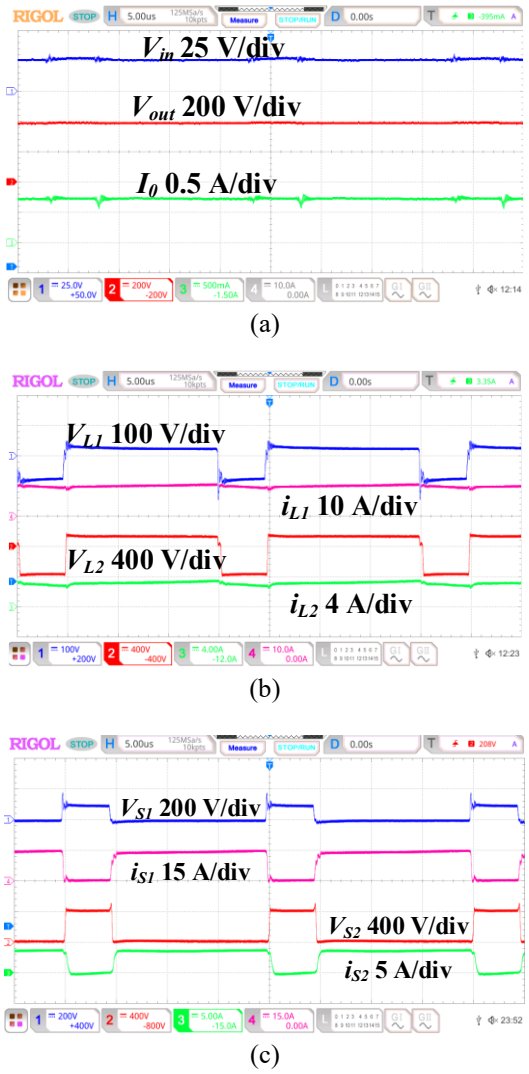

Fig. 13. Experimental results of 25V input 300W load (a) input voltage (VIn), output voltage (Vout), and current (I0), (b) Inductor voltages and currents, (c) Switch voltages and currents.

To further validate the performance of the proposed PMQBB converter, experimentation was conducted under varying input voltage and load conditions. The measured results confirm the converter's ability to maintain a regulated output voltage and continuous conduction mode across different inputs and loads. Specifically, the converter was tested at 40 V input with a 200 W load, 25 V input with a 300 W load, and 60 V input with a 300 W load. The corresponding efficiencies were observed as 95.8%, 94.2%, and 96.2%, respectively.

These performance metrics closely align with the theoretical calculations, confirming the converter's high voltage gain and efficiency under dynamic conditions. The experimental waveforms are shown in Figs. 12, 13, and 14 illustrate the converters steady-state performance under different input voltages and load levels.

V. Discussion on Advantages and Limitations

The proposed P-type Modified Quadratic Boost (PMQB) converter provides several notable advantages for DC microgrid applications. These include achieving a high voltage gain at moderate duty ratios, maintaining a continuous input current, ensuring a common ground between input and output, and utilizing fewer components compared to traditional multistage boost converters. Despite these strengths, the topology has a few limitations. The input current ripple is relatively higher, but this can be effectively minimized by increasing the inductance of L_1. In the proposed converter, the output diode D_0 is subjected to elevated voltage stress, as it must withstand both the output voltage and the voltage across L_2.To ensure reliable operation, wide-bandgap (WBG) diodes such as those based on silicon carbide (SiC) are employed, as they offer fast switching, high voltage tolerance, and better thermal performance compared to conventional silicon devices. However, this choice involves a practical trade-off. While SiC diodes contribute to improved

efficiency and reduced switching losses, they are generally more expensive and may necessitate specialized packaging and enhanced thermal management. Therefore, the selection of D_0 must account for these factors to achieve an optimal balance between performance, cost, and thermal reliability based on the specific application requirements.

Overall, these limitations are well within manageable design boundaries and do not detract from the converter's suitability for high-gain DC microgrid applications.

TABLE. I
COMPARATIVE ANALYSIS OF PMQBB CONVERTER VERSUS OTHER NON-ISOLATED CONVERTERS

REF	Voltage Gain	C/D/L/S	Component count	Order	Power Density	Control complexity	TCVS$\left(\frac{\sum V_C}{V_0}\right)$	PSVS$\left(\frac{\hat{V}_S}{V_0}\right)$	NSVS	*f/P/η (%)*
19	$\frac{D^2}{(1-D)^2}$ $D=\frac{G-\sqrt{G}}{G-1}$	3/2/3/2	10	6	Low	High	$\frac{1+D}{D}$	$\frac{1}{D}$	$\frac{1}{D^2}$	50kHz/100W/92
21	$\frac{\frac{1+D}{(1-D)^2}}{D=\frac{2G+1-\sqrt{8G+1}}{2G}}$	4/4/3/1	12	7	High	High	$\frac{4+3D+D^2}{(1+D)^2}$	$\frac{1}{1+D}$	$\frac{1}{1+D}$	100kHz/300W/82
22	$\frac{D^2}{(1-D)^2}$ $D=\frac{G-\sqrt{G}}{G-1}$	3/5/3/1	12	6	High	High	$\frac{1+D^2}{D^2}$	$\frac{1}{D^2}$	$\frac{1}{D^2}$	40kHz/300W/82
23	$\frac{D}{(1-D)^2}$ $D=\frac{2G+1-\sqrt{4G+1}}{2G}$	3/2/3/2	10	6	Low	High	$\frac{1+2D}{D}$	$\frac{1}{D}$	$\frac{2-D}{D}$	10kHz/60W/84
24	$\frac{1+D}{D(1-D)}$ $D=\frac{G-1-\sqrt{G^2-6G+1}}{2G}$	3/3/2/2	10	5	High	Moderate	$\frac{1+2D}{1+D}$	$\frac{1}{1+D}$	1	10kHz/280W/94.2
27	$\frac{2D(2-D)}{(1-D)^2}$ $D=\frac{\sqrt{G+2}-2}{\sqrt{G+2}}$	5/3/4/2	14	9	Low	High	$\frac{2+5D-3D^2}{2D(2-D)}$	$\frac{1}{2D(2-D)}$	$\frac{1}{2D}$	40kHz/160W/94.7
29	$\frac{2D}{(1-D)^2}$ $D=\frac{\sqrt{2G+1}-G+1}{G}$	3/3/2/2	10	5	Moderate	Moderate	$\frac{1}{D}$	$\frac{1+D}{2D}$	$\frac{1}{D}$	100kHz/110W/89
Topologies with the same gain										
28	$\frac{D(2-D)}{(1-D)^2}$ $D=\frac{G+1-\sqrt{G+1}}{G+1}$	3/2/3/2	10	6	Low	High	$\frac{1}{D}$	$\frac{1}{D(2-D)}$	$\frac{1}{D}$	64kHz/72W/91.8
30	$\frac{D(2-D)}{(1-D)^2}$ $D=\frac{G+1-\sqrt{G+1}}{G+1}$	3/2/3/2	10	5	High	Moderate	$\frac{1+3D-2D^2}{D(2-D)}$	$\frac{1}{D(2-D)}$	$\frac{1}{D}$	50kHz/200W/94
31	$\frac{D(2-D)}{(1-D)^2}$ $D=\frac{G+1-\sqrt{G+1}}{G+1}$	2/3/2/1	8	4	Low	Low	$\frac{1}{2-D}$	$\frac{1}{D(2-D)}$	$\frac{1}{D}$	64kHz/49W/90.8
Proposed PMQBB	$\frac{D(2-D)}{(1-D)^2}$ $D=\frac{G+1-\sqrt{G+1}}{G+1}$	2/2/2/2	8	4	High	Low	$\frac{1+D-D^2}{D(2-D)}$	$\frac{1}{D(2-D)}$	$\frac{1}{D}$	50kHz/300W/95.8

 # C= capacitors, D= diodes, L= inductors, S= switches, TCVS= total capacitor voltage stress, PSVS= peak switch voltage stress, NSVS= normalized switch voltage stress, f= switching frequncy, P= power , η= efficiency.

VI. CONCLUSION

This paper presents a P-type Modified Quadratic Buck-Boost Converter (PMQBB**)** converter featuring a p-type structure with a quadratic boost configuration. The proposed converter is thoroughly analysed and validated through a hardware prototype for 300W experimentation under Continuous Conduction Mode (CCM) gives a 400V output with 40V input. This analysis includes detailed discussions on the operating modes, semiconductor components' voltage stress analysis, and the design considerations for inductors and capacitors. The PMQBB achieves a high voltage gain of 10 times with fewer element count. The proposed PMQBB converter demonstrates a unique

characteristic of operating as a buck converter when the duty ratio D≤0.2929. A simple PI controller is implemented, which generally has a lower bandwidth compared to more advanced controllers. Experimental results demonstrate effective disturbance rejection for variations in load and input. This was accomplished without increasing computational complexity, confirming it as a practical and efficient control approach. Performance analysis reveals that the PMQBB offers continuous input current and significantly reduced inductor current ripple, ensuring enhanced efficiency of 95.8%. These attributes establish the proposed topology as an effective solution for high-gain DC-DC conversion applications.

TABLE II
HARDWARE CIRCUIT PARAMETERS

Specification	rating
V_{in}	40 V
v_{out}	400 V
Power rating (P)	300 W
Inductors	L_1= 1mH, L_2= 3mH (R_{L1}=R_{L2}=20mΩ)
Capacitors	C_0=100 µF,C_1= 22 µF (R_{c1}=1 mΩ, R_{c0}=0.1Ω)
Switches	NVHL027N65S3F (R_{DS}=27mΩ)
Diodes	D_1 & D_0=FFSH2065B (V_f=1.5 V, R_d = 10 mΩ)
Switching frequency	50kHz

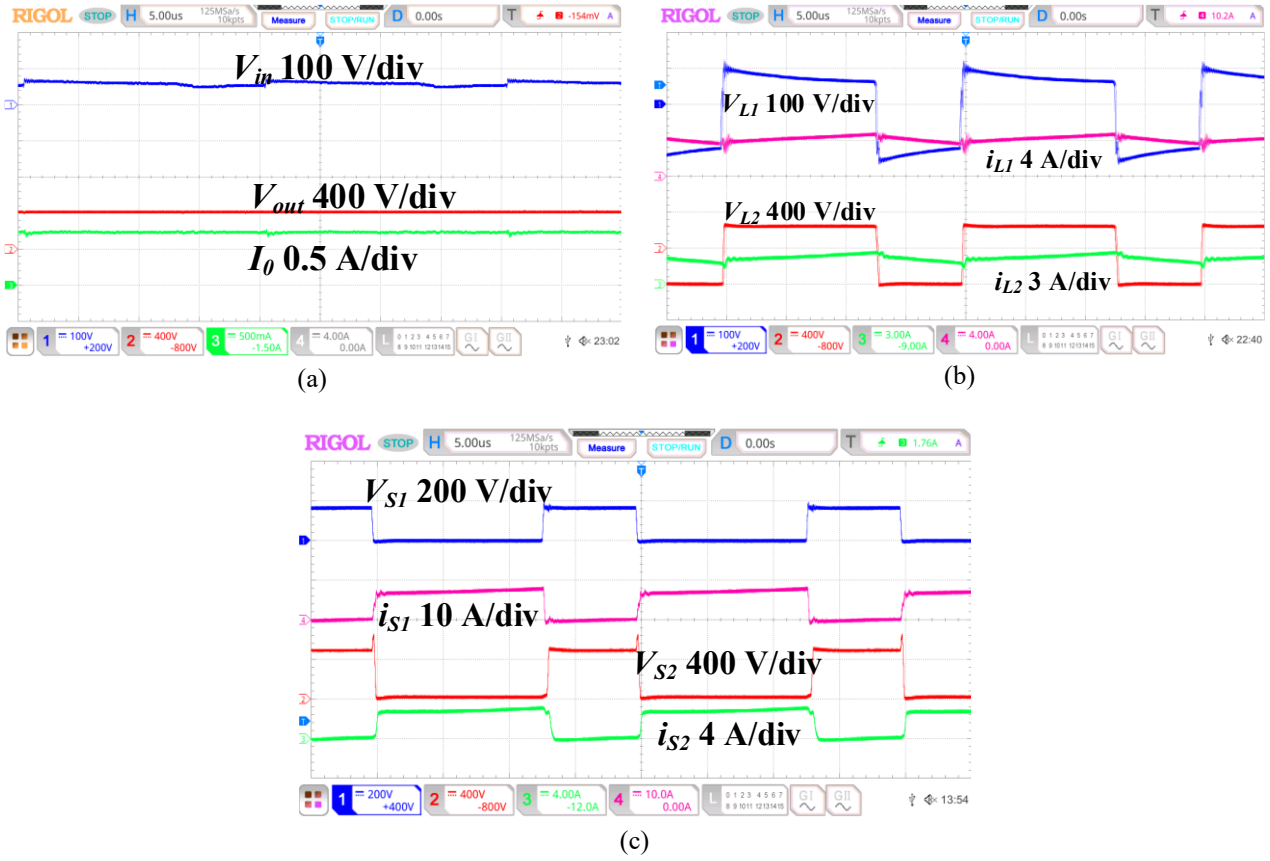

Fig. 14. Experimental results of 60V input 300W load (a) input voltage (VIn), output voltage (Vout), and current (I0), (b) Inductor voltages and currents, (c) Switch voltages and currents.

REFERENCES

[1] Renewable Energy Policy Network for the 21st Century (REN21), "Press Release: COP28 Sent Strong Signals for the Energy Transition but Much Work Lies Ahead to Set It on Course for a Fossil-Free and Renewables-Based Economies by 2050", 13 December 2023.

[2] K.. -W. Ma and Y.. -S. Lee, "A novel uninterruptible DC-DC converter for UPS applications," in *IEEE Transactions on Industry Applications*, vol. 28, no. 4, pp. 808-815, July-Aug. 1992, doi: 10.1109/28.148446.

[3] K. Modepalli, A. Mohammadpour, T. Li and L. Parsa, "Three-Phase Current-Fed Isolated DC–DC Converter With Zero-Current Switching," in *IEEE Transactions on Industry Applications*, vol. 53, no. 1, pp. 242-250, Jan.-Feb. 2017, doi: 10.1109/TIA.2016.2601297.

[4] A. Thiyagarajan, S. G. Praveen Kumar and A. Nandini, "Analysis and comparison of conventional and interleaved DC/DC boost converter," *Second International Conference on Current Trends In Engineering and Technology - ICCTET 2014*, Coimbatore, India, 2014, pp. 198-205, doi: 10.1109/ICCTET.2014.6966287.

[5] B. L. Narasimharaju, S. P. Dubey, and S. P. Singh, "Design and analysis ofcoupled inductor bidirectional DC-DC convertor for high-voltage diversity applications," IET Power Electron., vol. 5,

no. 7, pp. 998–1007, Aug. 2012, https://doi.org/10.1049/iet-pel.2011.0141.

[6] Naresh SVK, Peddapati S. Complementary switching enabled cascaded boost-buck-boost (BS-BB) and buck-boost-buck (BB-BU) converters. Int J Circ Theor Appl. 2021; 49(9): 2736–2753. https://doi.org/10.1002/cta.3034

[7] A. Ebrahimi, E. Babaei and V. Ranjbarizad, "Voltage Balancing of Diode-Clamped Multilevel Converter by Using Modified Quasi-Z-Source Network," 2019 4th International Conference on Power Electronics and their Applications (ICPEA), Elazig, Turkey, 2019, pp. 1-6, doi: 10.1109/ICPEA1.2019.8911163.

[8] Baba MF, Giridhar AV, Narasimharaju BL. Active switched-capacitor based ultra-voltage gain quadratic boost DC-DC converters. Int J Circ Theor Appl. 2022;1 – 28. doi:10.1002/cta.

[9] S. Gao, Y. Wang and D. Xu, "Modified SEPIC Converter With High Voltage Gain and ZVS Characteristics," in IEEE Transactions on Circuits and Systems II: Express Briefs, vol. 66, no. 11, pp. 1860-1864, Nov. 2019, doi: 10.1109/TCSII.2018.2890688.

[10] V. Seshagiri Rao and K. Sundaramoorthy, "Performance Analysis of Voltage Multiplier Coupled Cascaded Boost Converter With Solar PV Integration for DC Microgrid Application," in IEEE Transactions on Industry Applications, vol. 59, no. 1, pp. 1013-1023, Jan.-Feb. 2023, doi: 10.1109/TIA.2022.3209616.

[11] Allehyani, A., Alsolami, M. Two Leg Dual Inductor Hybrid Step-Up DC/DC Power Converter for Renewable Energy Resources. J. Electr. Eng. Technol. 17, 2857–2865 (2022). https://doi.org/10.1007/s42835-022-01090-7

[12] B. Faridpak, M. Bayat, M. Nasiri, R. Samanbakhsh and M. Farrokhifar, "Improved Hybrid Switched Inductor/Switched Capacitor DC–DC Converters," in IEEE Transactions on Power Electronics, vol. 36, no. 3, pp. 3053-3062, March 2021, doi: 10.1109/TPEL.2020.3014278.

[13] Y. Tang, T. Wang and D. Fu, "Multicell Switched-Inductor/Switched-Capacitor Combined Active-Network Converters," in IEEE Transactions on Power Electronics, vol. 30, no. 4, pp. 2063-2072, April 2015, doi: 10.1109/TPEL.2014.2325052.

[14] Baba MF, Giridhar AV, Narasimharaju BL. Nonisolated high gain hybrid switched-inductor DC-DC converter with common switch grounding. Int J Circ Theor Appl. 2022;1 - 19. doi:10.1002/cta.3295

[15] S. Miao, W. Liu and J. Gao, "Single-Inductor Boost Converter With Ultrahigh Step-Up Gain, Lower Switches Voltage Stress, Continuous Input Current, and Common Grounded Structure," in IEEE Transactions on Power Electronics, vol. 36, no. 7, pp. 7841-7852, July 2021, doi: 10.1109/TPEL.2020.3047660.

[16] Kanithi AK, B L N. A wide voltage range non-isolated continuous input buck-boost converter for optimal green energy harvesting in LED lighting systems. Int J Circ Theor Appl. 2024;1-31. doi:10.1002/cta.4238

[17] B. F. Monakanti, G. Archakam Vijayaraghavulu, N. Beeramangalla Lakshminarasiah and H. Sarma Krishnamoorthy, "An Ultra High Gain Switched-Capacitor Boost DC-DC converter with Reduced Ripple Current," in IEEE Latin America Transactions, vol. 22, no. 11, pp. 920-932, Nov. 2024, doi: 10.1109/TLA.2024.10735444.

[18] Naresh SVK, Peddapati S, Alghaythi ML. A non-isolated high quadratic step-up converter for fuel cell electric vehicle applications. Int J Circ Theor Appl. 2023; 51(8): 3841-3864. doi:10.1002/cta.3610.

[19] H. Gholizadeh, S. A. Gorji and D. Sera, "A Quadratic Buck-Boost Converter With Continuous Input and Output Currents," in *IEEE Access*, vol. 11, pp. 22376-22393, 2023, doi: 10.1109/ACCESS.2023.3253102.

[20] S. V. K. Naresh, H. Shareef, B. Kumar and S. Peddapati, "An Ultra High Gain Quadratic Boost Converter with Reduced Electric Stress for Photovoltaic Applications," in *IEEE Transactions on Industry Applications*, doi: 10.1109/TIA.2025.3550107.

[21] J. Leyva-Ramos, R. Mota-Varona, M. G. Ortiz-Lopez, L. H. Diaz-Saldierna and D. Langarica-Cordoba, "Control Strategy of a Quadratic Boost Converter With Voltage Multiplier Cell for High-Voltage Gain," in IEEE Journal of Emerging and Selected Topics in Power Electronics, vol. 5, no. 4, pp. 1761-1770, Dec. 2017, doi: 10.1109/JESTPE.2017.2749311.

[22] N. Zhang, G. Zhang, K. W. See and B. Zhang, "A Single-Switch Quadratic Buck–Boost Converter With Continuous Input Port Current and Continuous Output Port Current," in IEEE Transactions on Power Electronics, vol. 33, no. 5, pp. 4157-4166, May 2018, doi: 10.1109/TPEL.2017.2717462.

[23] Okati, M., Eslami, M., Jafari Shahbazzadeh, M., Shareef, H.: A new transformerless quadratic buck–boost converter with high-voltage gain ratio and continuous input/output current port. IET Power Electron. 15, 1280–1294 (2022). https://doi.org/10.1049/pel2.12304

[24] Mohammadzadeh Shahir, F., Babaei, E., Sabahi, M.: A new expandable non-isolated opposite polarity boost DC–DC converter with fewer switches. IET Power Electron. 15, 1699–1712 (2022). https://doi.org/10.1049/pel2.12339

[25] M. F. Baba, A. V. Giridhar and B. L. Narasimharaju, "A Wide Voltage Range Bidirectional High Voltage Transfer Ratio Quadratic Boost DC-DC Converter for EVs With Hybrid Energy Sources," in IEEE Journal of Emerging and Selected Topics in Industrial Electronics, vol. 5, no. 2, pp. 521-530, April 2024, doi: 10.1109/JESTIE.2023.3327639.

[26] P. Raviteja, K. A. Kumar, M. F. Baba, B. L. Narasimharaju and A. V. Giridhar, "A Modified Quadratic Boost Based P-Type Structure with Inverting Output," 2024 IEEE 4th International Conference on Sustainable Energy and Future Electric Transportation (SEFET), Hyderabad, India, 2024, pp. 1-5, doi: 10.1109/SEFET61574.2024.10718216.

[27] K. Yari, S. H. Shahalami and H. Mojallali, "A Novel Nonisolated Buck–Boost Converter With Continuous Input Current and Semiquadratic Voltage Gain," in *IEEE Journal of Emerging and Selected Topics in Power Electronics*, vol. 9, no. 5, pp. 6124-6138, Oct. 2021, doi: 10.1109/JESTPE.2021.3069788.

[28] Okati, M., Eslami, M. & Khan, B. A novel semi-quadratic buck-boost structures with continuous input current for PV application. *Sci Rep* 14, 14134 (2024). https://doi.org/10.1038/s41598-024-65012-5

[29] A. Sarikhani, B. Allahverdinejad and M. Hamzeh, "A Nonisolated Buck–Boost DC–DC Converter With Continuous Input Current for Photovoltaic Applications," in *IEEE Journal of Emerging and Selected Topics in Power Electronics*, vol. 9, no. 1, pp. 804-811, Feb. 2021, doi: 10.1109/JESTPE.2020.2985844.

[30] Hosseinpour, M. and Dastgiri, A. (2023). A new positive output high gain quadratic buck-boost converter: analysis, design and control. Jordan Journal of Electrical Engineering, 9(2), 189. https://doi.org/10.5455/jjee.204-1670524690

[31] Gorji, S.A., Mostaan, A., Tran My, H. and Ektesabi, M. (2019), Non-isolated buck–boost dc–dc converter with quadratic voltage gain ratio. IET Power Electronics, 12: 1425-1433. https://doi.org/10.1049/iet-pel.2018.5703

P. Raviteja (Graduate Student Member, IEEE) received his B.Tech and M.Tech degrees in Electrical Engineering from Jawaharlal Nehru Technological University, Hyderabad,Telangana, India, in 2012 and 2015, respectively. He is currently pursuing Ph.D. degree in Electrical Engineering at the National Institute of Technology Warangal, Telangana, India. His research interests include switched-mode power supplies and high-gain DC–DC converters.

B. L. Narasimharaju (S'10, M'12 and SM'16) (Senior Member, IEEE) received his B.E. in electrical engineering, and M.E degrees in Power Electronics, from University Visvesvaraya College of Engineering (UVCE), Bangalore, India, in 1999 and 2002 respectively, and the Ph.D degree from the Indian Institute of Technology Roorkee (IIT Roorkee), Roorkee, India, in 2012. He worked as Project Trainee at ABB Bangalore, India from March 2001 to August 2001, and since then till March 2002, he worked at LRDE, Ministry of Defense, India. He was a Teaching Assistant with UVCE from 2002 to 2003. From 2003 to 2012, he was a Faculty of Electrical Engineering at Manipal Institute of Technology (MIT), Manipal University, Manipal, India. Currently, he is a Professor of Electrical Engineering, National Institute of Technology Warangal, India. His research credential includes, executed funded research projects worth of 3.50 crores, 09 Ph.D guidance, more than 100 research publications. His research interests include power converter design, control, electric drives, implementation, and applications in rural & urban community relevance.

S. V. K. Naresh (Member, IEEE) received his B.Tech degree in Electrical and Electronics Engineering from Jawaharlal Nehru Technological University Kakinada, India, in 2015, and his M.Tech degree in Power Electronics and Power Systems from the National Institute of Technology Goa, India, in 2017. He earned his Ph.D. in Electrical Engineering from the National Institute of Technology Andhra Pradesh, India, in 2023. Following his doctoral studies, he served as a Postdoctoral Fellow at the National Water and Energy Center, United Arab Emirates University, Al Ain, UAE, from August 2023 to October 2024. He later worked as a Senior Engineer at CastNX Pvt. Ltd., Indore, India, from Dec 2024 to May 2025. He is currently working as an Assistant Professor in the Department of Electrical and Electronics Engineering at SRM University Andhra Pradesh, India. His research interests include high-gain DC-DC converters, microinverters, fault-tolerant multilevel inverters, and reliability assessment of power converters.